Discover Mechanical Engineering

RESEARCH Open Access

Interpretable weld quality prediction in ultrasonic metal welding using change point detection

Oliver Stockemer[1*], Eric Helfers[2], Elson Pinto[1], Alexander Schiebahn[2], Uwe Reisgen[2] and Burkhard Corves[1]

*Correspondence:
Oliver Stockemer
stockemer@igmr.rwth-aachen.de
[1]Institute of Mechanism Theory, Machine Dynamics and Robotics (IGMR), RWTH Aachen University, Eilfschornsteinstraße 18, 52062 Aachen, Germany
[2]Welding and Joining Institute (ISF), RWTH Aachen University, Pontstraße 49, 52062 Aachen, Germany

Abstract

Ultrasonic metal welding is a widely used process for joining metals to create electrical connections using high-frequency mechanical vibrations. Despite its industrial relevance, achieving consistent joint quality remains challenging and requires a deeper understanding of the relationship between process parameters and joint quality. The challenge here is identifying the process signals that significantly correlate with the joint quality. Due to the nature of the process, manual evaluation of such signals is ineffective, leading to an increased focus on implementing statistical or machine learning-based models for predicting joint quality. This study proposes a method to improve the accuracy and interpretability of predicting joint quality using machine learning models. Welding experiments involving various machine internal and external sensors are conducted. The sensors' measurement data are recorded synchronously as time series. Since most machine learning models require scalar input, informative features must be extracted from the time series data. Various statistical and signal-based features can be extracted from the entire time series. To distinguish between the influences of the different process phases and their overall behavior, the signals are divided into segments. Although equal-length segmentation is simple, it overlooks signal characteristics such as steep transitions or prolonged steady states. Change point detection enables segmentation based on signal behavior, allowing for more relevant feature extraction. Moreover, the detected segments can be associated with known process phases, linking data-driven insights with domain knowledge. As a result, both the predictive performance and interpretability of the ML models improve, allowing for clearer associations between process phases and quality outcomes.

Keywords Ultrasonic metal welding, Quality prediction, Machine learning, Change point detection

1 Introduction

Ultrasonic metal welding (USMW) is becoming increasingly important in industrial practice and plays a central role in several emerging technological fields. As a solid-state joining method with low heat input, USMW enables the reliable connection of highly

© The Author(s) 2026. **Open Access** This article is licensed under a Creative Commons Attribution 4.0 International License, which permits use, sharing, adaptation, distribution and reproduction in any medium or format, as long as you give appropriate credit to the original author(s) and the source, provide a link to the Creative Commons licence, and indicate if changes were made. The images or other third party material in this article are included in the article's Creative Commons licence, unless indicated otherwise in a credit line to the material. If material is not included in the article's Creative Commons licence and your intended use is not permitted by statutory regulation or exceeds the permitted use, you will need to obtain permission directly from the copyright holder. To view a copy of this licence, visit http://creativecommons.org/licenses/by/4.0/.

conductive materials, such as copper and aluminum, which are fundamental to modern energy and mobility systems. USMW is particularly widespread in battery cell production, power electronics, and wiring harness assembly in electric vehicles.

Beyond its technical advantages, USMW contributes to broader sustainability objectives. Its material efficiency, low energy consumption, and capability to join dissimilar metals support European industry's transition toward climate-neutral manufacturing. [1]

In USMW, the parts to be joined are pressed together in an overlapping configuration under a defined normal force and bonded through high-frequency mechanical vibrations without reaching the melting point. A high-frequency generator produces an alternating voltage, which is converted into mechanical oscillations by the converter. These vibrations are transmitted through the booster and sonotrode to the workpiece surface at a typical frequency of 20 kHz. Simultaneously, the anvil acts as a counter bearing, constraining the motion of the lower workpiece and ensuring proper fixation during the joining process. The combination of frictional sliding, plastic deformation, and surface activation leads to the formation of a solid-state metallurgical bond, typically assessed through mechanical testing such as tensile shear or peel tests. As demonstrated in the works of de Vries [2] and Balz [3], this bond formation consists of multiple process phases.

Although USMW is an established industrial process [3, 4], achieving consistently high weld quality remains challenging due to its strong sensitivity to disturbances [5]. A wide range of machine- and component-dependent influences affect the joining behavior, including tool wear of the sonotrode and anvil, parameter drift, material hardness, surface condition, contamination, and geometric tolerances of the sheets. Many of these factors interact in complex, often nonlinear ways, and comprehensive physical process models are still lacking [6]. As a result, significant fluctuations in weld quality may occur even when nominal parameters are held constant, particularly during material batch changes or when surface conditions vary [3, 7, 8].

Because 100% non-destructive testing is not yet reliably possible and random destructive testing is costly, industrial practice typically relies on statistical process monitoring, such as evaluating welding time or sonotrode penetration within process windows, combined with random destructive testing [9, 10]. However, these indirect methods cannot ensure that each individual weld meets the required strength [2, 6]. Consequently, defective welds may remain undetected, while large numbers of acceptable welds are sometimes discarded as a precaution when individual failures occur. This results in unnecessary material waste and supports the need for predictive, non-destructive, inline monitoring techniques capable of linking process signals directly to weld quality.

Machine learning (ML) has therefore gained increasing attention in recent years. ML methods can identify and link complex temporal patterns in process signals to weld quality. Several studies have demonstrated that data-driven models significantly outperform traditional, purely scalar monitoring approaches [7, 11]. Müller et al. extract scalar features from either the full signal or predefined, equally sized time intervals to make use of the rich information contained in time series sensor data [12]. These features are then used as input for ML algorithms, such as Random Forests, Extremely Randomized Trees, Support Vector Machines, and gradient-boosted ensembles, which have shown promising predictive performance [11].

However, despite these advances, important limitations remain. Recent methods apply fixed, equal-length segmentation to measurement signals, which does not align with the true phase-dependent dynamics of the USMW process. Physical transitions, like softening and bond formation, occur at different times and durations, depending on the material and process conditions. When these transitions cut across segment boundaries, the resulting features lose representativeness and may obscure meaningful changes in the underlying signal. Consequently, the interpretability of ML models suffers because influential features cannot be clearly assigned to specific process phases, and the link between signal changes and weld quality remains difficult to understand. This transforms many ML models into black boxes rather than tools that provide actionable insight into the process.

The limitations of fixed, equal-length segmentation highlight a central methodological gap in current data-driven approaches to weld quality prediction.

Balz introduced a detailed process phase model that divides the USMW process into six characteristic stages [3], underscoring the inherently phase-dependent nature of bond formation. However, existing data-driven monitoring techniques do not explicitly incorporate these phase-dependent variations. As a result, signal segments often cut across physical process transitions, reducing feature relevance and obscuring the relationship between process behavior and weld quality.

Motivated by this gap, this study introduces an adaptive segmentation method that responds to statistical changes in the sensor signals rather than relying on fixed temporal boundaries. Unlike many existing applications of change-point detection, which primarily use statistical change points to signal anomalies or abnormal intervals in time series data rather than to segment processes into their physical phases [13], change-point detection is here integrated directly into the feature engineering pipeline for adaptive segmentation.

The objective of this study is to improve weld quality prediction in USMW by introducing an adaptive, data-driven segmentation approach based on statistical change-point detection. To the authors' knowledge, this is the first study to integrate change-point-based segmentation directly into the feature engineering stage of ML-based weld quality prediction in ultrasonic metal welding.

To address this, the study contributes the following:

- Adaptive signal segmentation using change point detection: Instead of dividing signals into predefined intervals, the proposed method detects statistical changes in the time series, producing segments that reflect true process behavior.
- Integration of multi-sensor time series: Change point detection is applied across multiple machine-internal and external sensor signals to reveal consistent transitions in the process.
- Extraction of segment-based features: Statistical features are computed for each adaptively identified segment, enabling a more accurate representation of the underlying process dynamics.
- Machine learning pipeline based on Extra Trees: An ExtraTreesRegressor is trained using scikit-learn to predict the tensile shear strength of the welds.
- Interpretability through permutation importance: Feature importance analysis links influential features to specific, physically meaningful process phases, improving transparency and understanding of the weld formation mechanisms.

Table 1 Parameters of the welding process (machine settings in brackets)

Parameter	Parameter set 1 (Reference)	Parameter set 2
Force	625 N (1.25 bar)	1625 N (3.25 bar)
Amplitude	30 μm (110%)	24 μm (80%)
Energy	1600 J	750 J

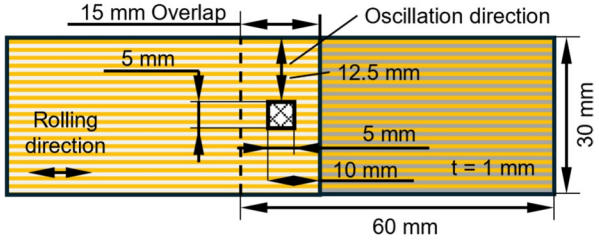

Fig. 1 Specimen geometry

- Demonstration of improved predictive performance: The study shows that change-point-based segmentation yields more accurate and interpretable quality predictions than conventional equal-length segmentation.

In summary, this work provides a methodology that bridges data-driven analysis with domain-specific process knowledge, demonstrating that segmenting sensor signals according to their intrinsic statistical structure leads to more reliable and interpretable weld quality prediction.

The following work is organized as follows: Sect. 2 describes the experimental setup and data acquisition. Section 3 presents the proposed methodology, including adaptive segmentation and feature extraction. Section 4 discusses the results, including weld quality prediction and interpretability analysis. Finally, Sect. 5 concludes the study and outlines potential future work.

2 Experimental setup

The experiments were conducted using an industry-standard 4 kW welding system (Schunk LS-C) with an operating frequency of approximately 20 kHz. The schematic structure of the machine was introduced in Sect. 1 and is shown in Fig. 2. The process is controlled via energy. Additionally, the amplitude of vibration at the sonotrode and the normal force applied to the workpieces need to be determined. These parameters are determined based on standard practice using parameter studies (design of experiment-DOE). Two parameter sets were defined. The reference parameter set is summarized in Table 1. A second parameter set was additionally investigated to evaluate the influence of increased force and amplitude.

For the welding tests, electrolytic tough pitch cold-rolled copper plates (Cu-ETP) with a thickness of 1 mm are used. Two plates with the dimensions of 60 x 30 mm are welded on a spot of 5 x 5 mm with a 15 mm overlap. The geometry is shown in Fig 1.

The objective of these experiments is to investigate the influence of a broad range of external factors on the USMW process. To this end, several test groups have been defined. Within each group, including the reference group, welds were produced using parameter set 1 or parameter set 2. The reference group (R) establishes a baseline for standard process behavior. This group uses half-hard copper (Cu-ETP R240), does not

undergo additional cleaning, and pneumatic clamping is used to ensure precise positioning without shifting during welding. This study conducted 476 welds for this group. Seven additional groups were defined to systematically investigate the influence of material properties and process variations representative of industrial practice. Group S investigates the influence of reduced material hardness using soft copper (Cu-ETP R220) (221 welds). Group H employs a harder copper material (Cu-ETP R290) while keeping all other conditions unchanged (126 welds). Group F introduces surface contamination by applying a thin layer of different oils and greases between the joining partners prior to welding (246 welds). This leads to reduced surface friction. In group C, the specimens undergo chemical cleaning in an ultrasonic bath with 2-propanol, after which the solvent evaporates (75 welds). Group A examines the influence of surface modification by mechanically roughening the sheets using an abrasive fleece (45 welds). Group X investigates the effect of omitting pneumatic clamping during welding (42 welds). Group O comprises additional industrially relevant variations that do not fall into the previously defined categories (41 welds). In total, 796 welds were produced within the additional test groups, resulting in an overall dataset of 1272 welding experiments.

These variations represent plausible industrial conditions and were deliberately selected to amplify potential influences on the welding process. Table 2 summarizes the test groups.

The selection of sensors in this study is based on two criteria: achieving the most comprehensive mapping possible of the ultrasonic metal welding process and using sensors representative of industrial practice. As shown in Fig. 2, a total of six analog voltage-based measurement signals are recorded. All signals are digitized using a National Instruments data acquisition system with a simultaneous sampling rate of 500 kS/s per channel. This high sampling rate ensures accurate capture of the ultrasonic working frequency of 20 kHz and its higher harmonics. The measurement software synchronizes all channels at the start of each weld.

The electrical power signal of the ultrasonic generator is monitored to capture the energy input and determine the start and end of the welding cycle. A strain gauge-based force sensor, which is integrated into the piston rod of the pneumatic cylinder, records the normal force applied during weld formation. Due to the indentation of the sonotrode into the workpieces, the force is not constant. It temporarily decreases as the material softens and undergoes plastic deformation. The machine compensates for this by adjusting the pneumatic pressure. The indentation depth is measured using a linear variable differential transformer (LVDT).

Table 2 Overview of the weld specimen configurations

Test series	Additional information	Base material	Treatment	Count [-]
R	Reference (foil clean)	Cu-ETP R240	EXW	476
S	Soft	Cu-ETP R220	EXW	221
H	Increased hardness	Cu-ETP R290	EXW	126
F	Contamination	Cu-ETP R240	1:100 grease dilution	246
C	Chemically cleaned	Cu-ETP R240	2-Propanol	75
A	Roughened	Cu-ETP R240	abrasive fleece	45
X	Without clamping	Cu-ETP R240	EXW	42
O	Other	Cu-ETP R240	other	41
Total				1272

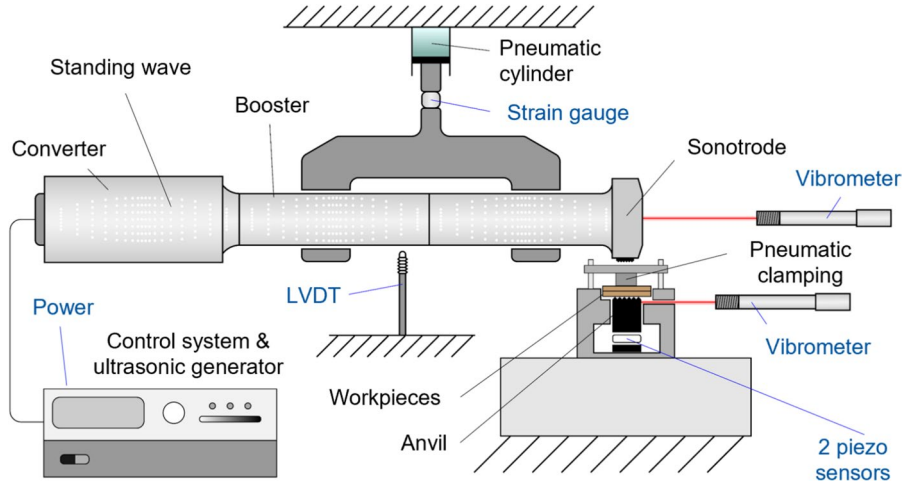

Fig. 2 Schematic structure of an USMW system: experimental setup and sensor equipment

Two laser vibrometers are used within the setup. One is a Polytec VibroFlex Xtra VFX-I-120 targeted on the sonotrode to measure its excitation. The other is a Polytec VibroFlex QTec VFX-I-160 targeted at the anvil. The latter serves as a reference signal to validate the performance of the integrated shear-force sensors in the anvil. Recent work has demonstrated that shear-force measurements obtained with this sensor-integrated anvil design closely reproduce the dynamic amplitude and frequency response measured by laser vibrometers at the anvil, yielding a mean coefficient of determination of $R^2 \approx 0.99$ across 175 welding experiments under varying process conditions, while offering a more robust and industrially integrable alternative to laser-based measurements [14]. Consequently, all subsequent analyses rely on the shear-force sensor rather than the vibrometer to characterize the anvil vibration. The piezoelectric shear-force sensors are connected to a summing box, and their combined charge signal is converted into a proportional voltage signal via a Kistler 5015A laboratory charge amplifier.

In total, these synchronized measurements provide a comprehensive representation of both the excitation introduced by the sonotrode and the dynamic reaction of the workpieces and anvil, enabling detailed process analysis across varying welding conditions.

After the welding experiments, the quality of the specimens must be determined. The mechanical tensile shear force is used as an indicator of quality for the connection.

3 Methodology

This chapter presents the data-driven workflow for predicting weld quality in USMW. The methodology covers the entire process, from raw sensor signals to the final tensile shear strength prediction. First, the raw measurements are preprocessed systematically to eliminate noise and extract relevant frequency components. Next, change point detection divides the signals into meaningful segments that reflect the dynamic evolution of the welding process. A comprehensive set of statistical and temporal features is then extracted from these segments. These features then serve as input for a supervised ML model that predicts weld strength and provides insight into the most influential process characteristics.

3.1 Data preprocessing

The sensors presented in the previous chapter provide raw measurement signals that require processing before further evaluation. First, the recorded voltage values are converted into the corresponding physical units. Where necessary, such as with the LVDT sensor, an offset correction is applied. Next, the relevant frequency components are extracted from the noisy raw data. For vibration signals, the primary interest lies in the operating frequency of approximately 20 kHz and its first two higher harmonics at 40 kHz and 60 kHz, respectively. Due to the decreasing amplitudes of higher orders and the requirement for very high sampling rates, additional harmonics contribute limited value to the analysis.

To isolate these frequency components, fifth-order Butterworth bandpass filters are applied. Previous studies have shown that bandpass filtering achieves results comparable to significantly more computationally demanding methods, such as wavelet transformations [9]. Considering the requirements for future real-time or near-real-time process monitoring, where computational efficiency is critical, the simpler filtering approach is preferred. Since the operating frequency may fluctuate slightly during the welding process, the passband is intentionally widened to 1000 Hz.

In the final preprocessing step, the amplitude curve of the high-frequency vibration signals is extracted. To accomplish this, the signal envelope is calculated using a Hilbert transform [15]. The resulting envelope signal no longer contains high-frequency oscillatory components, which makes the original high sampling rate unnecessary. Consequently, the envelope is downsampled to reduce the amount of data and the computational load.

To further smooth the amplitude curve, a low-pass filter is applied. This removes low-frequency disturbances that arise in the area of the operating frequency band, ensuring a clean representation of the signal's overall amplitude trend. Figure 3 illustrates this processing chain using an example from the shear force sensor. It shows the raw signal, the bandpass-filtered signal, and the extracted envelope. The figure clearly demonstrates the strong amplitude reduction and smoothing effect of the filtering steps.

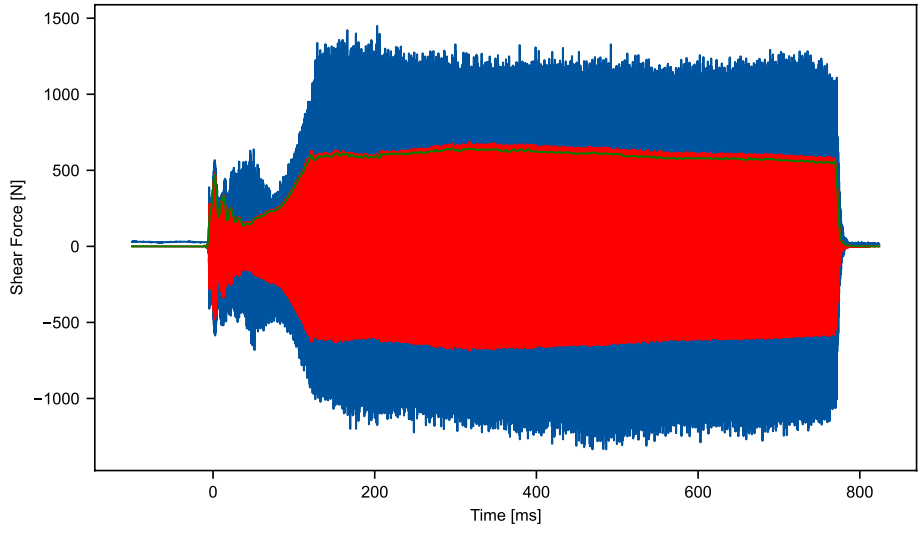

Fig. 3 Measurement data from the shear force sensor of an example measurement; blue: raw data, red: filtered data, green: envelope

Sensors that do not measure high-frequency vibrations, such as the strain gauge sensor or LVDT sensor, are also subjected to low-pass filtering to suppress noise. Additionally, all sensor signals must be examined for potential measurement errors. For example, optical sensors may be disturbed by particles passing through the measurement beam, and faulty wiring or defective components can introduce invalid data. Such corrupted signals must be detected and removed prior to process evaluation to avoid misleading predictions.

Even though the sensor signals are synchronized by the measurement device, small deviations in time and in the start of the weld can still occur. To make sure that each weld is exactly synchronized, the time 0 is set where the power signal has the value 0.2 kW. This is especially important in the feature calculation step, where the first segment could be influenced by deviations in start time. An overview of all preprocessing parameters is given in Table 3.

During experimental investigations, the measured normal force exhibited systematic day-dependent drifts, despite identical process parameter settings and constant pneumatic pressure levels. All welding experiments conducted within a single day showed a comparable force level, whereas measurements from different days were shifted by an approximately constant offset, with deviations reaching up to 12 % from the calculated nominal force value.

In this study, a dedicated reference group was evaluated, in which all welding experiments were performed using identical machine settings and process parameters. Therefore, no systematic variation of the mechanical process conditions is expected within this group. Despite the constant parameterization, the observed day-dependent offsets persist in the measured sensor signals. To evaluate whether these offsets have an influence on the actual joint quality, the resulting shear tensile strengths were analyzed for the same reference group. No systematic trend or correlation with the measurement day was observed. The mechanical performance of the welds thus remains unaffected by the observed signal offsets.

Based on these findings, the offsets are attributed to measurement- and system-related influences rather than process-induced effects. Consequently, the absolute signal level is not considered physically meaningful for the reference group. For this reason, the

Table 3 Overview of preprocessing filter settings and downsampling parameters

Signal	Filter type	Passband / cut-off (kHz)	Purpose
LVDT indentation	Low-pass	$f_c = 0.5$	Quasi-static displacement
Normal force	Low-pass	$f_c = 0.015$	Force trend extraction
Electrical power	Low-pass	$f_c = 0.4$	Energy input monitoring
Shear force	Band-pass	20–21	Fundamental frequency
Vibrometer (anvil)	Band-pass	20–21	Fundamental frequency
Vibrometer (sonotrode)	Band-pass	20–21	Fundamental frequency
Shear force	Band-pass	40–41	2nd harmonic
Vibrometer (anvil)	Band-pass	40–41	2nd harmonic
Vibrometer (sonotrode)	Band-pass	40–41	2nd harmonic
Shear force	Band-pass	60–61	3rd harmonic
Vibrometer (anvil)	Band-pass	60–61	3rd harmonic
Vibrometer (sonotrode)	Band-pass	60–61	3rd harmonic

Envelope extraction: Hilbert transform applied after band-pass filtering

Downsampling: Factor 500 (from 500 kS/s to 1 kS/s)

Synchronization: Power signal with value 0.2 at time 0

time-dependent sensor signals are normalized at the beginning of the process. The normalization is performed by computing the mean value of the normal force signal within the first 80 ms of the pre-weld preview phase and subtracting this value from the entire signal. This normalization removes the day-dependent offset while preserving the temporal signal evolution that contains the relevant process information.

3.2 Change point detection

Adaptive signal segmentation using change point detection is employed to better capture the true process behavior. Instead of dividing signals into predefined, equal-length segments, the proposed method detects statistical changes in the time series, producing segments that reflect phase-dependent dynamics. This addresses the question of how differences in time curves can be extracted as features for ML, since classical algorithms require scalar inputs [16]. Features are therefore extracted from the processed measurement data in a way that preserves the relevant signal characteristics.

Change point detection is the problem of identifying points in a time series where the underlying data distribution of the signal changes. In general, the problem can be modeled as follows:

$$x_1, x_2, \ldots, x_T; ; \rightarrow; ; \text{find } \tau_1, \tau_2, \ldots, \tau_K \text{ such that } P(x_t) \text{ changes at } \tau_i,$$

where $x_1, \ldots, x_T$ are time-series or signal samples, $\tau_1, \ldots, \tau_K$ are change points, and $P(x_t)$ is the unknown generating distribution.

Change point detection methods are typically divided into two categories: online detection methods, which detect real-time anomalies in signals, and offline detection methods, which detect changes after all samples have been received.

Initial work [17] in this field focused on statistical methods for detecting shifts in the mean of independently and normally distributed time series. Since then, approaches based on the Likelihood Ratio, Bayesian methods, and Maximum Likelihood Estimation have been described in the literature [18]. Modern approaches employ deep learning methods such as Neural Networks [19], Autoencoders [20], and LSTMs [21], which have shown strong results in detecting changes in real-world data. However, these methods often require large amounts of data.

In this study, *ruptures* [22] is used, a Python package for offline change point detection in multivariate time series. Ruptures provides a unifying framework for:

- Cost functions (linear models [L1, L2], kernel-based, maximum likelihood estimation, etc.)
- Search methods (exact [dynamic programming] and approximate [window-based, binary segmentation])
- Constraints (known and unknown number of change points)

The unifying nature, along with the straightforward implementation of various search methods and cost functions, makes ruptures an excellent choice for quick experimentation and comparison across different methods.

Here, ruptures is applied in three different ways to identify change points in the recorded sensor signals: univariate, multivariate, and hybrid. Each approach provides different insights into the underlying structure of the data and allows to assess the stability of the detected change points across signals.

In the univariate setting, ruptures is applied independently to each of the sensor signals. For each signal, a separate segmentation process is performed using the selected cost function and search method. This results in six distinct sets of change points, one for each signal. This approach allows to examine how each signal behaves individually and to identify signal-specific events or distributional shifts that may not be present in the other channels.

In the multivariate setting, all signals are jointly modeled as a multivariate time series. Ruptures is applied to the combined signal matrix, allowing the algorithm to detect change points that correspond to coordinated changes across multiple sensors. This approach captures system-level events that occur simultaneously across several channels and helps identify change points that are consistent at the multivariate level but may not be strongly expressed in any single signal.

In the hybrid approach, change points are identified using only one chosen signal, and the resulting set of change points is then applied to all the signals. This produces a common segmentation across the multivariate data, but the boundaries are derived from a single signal that is considered most informative or reliable for change point detection. This approach ensures alignment of segments across signals, enabling consistent downstream feature extraction while avoiding the computational cost and potential noise sensitivity of fully multivariate detection.

In this methodology, an exact algorithm based on Dynamic Programming (Dynp) is used to search for change points, as described in [22]. This algorithm first identifies an optimal change point using the specified cost function (which partitions the signal into sub-signals) and then recursively solves for the remaining change points within each resulting sub-signal.

The L2 cost function denoted as c_{L_2} is chosen based on preliminary tests. This cost function corresponds to the mean-shift model where each segment has constant mean and same variance. The cost function c_{L_2} is given by

$$c_{L_2}(y_{a..b}) := \sum_{t=a+1}^{b} \|y_t - \bar{y}_{a..b}\|_2^2 \tag{1}$$

where $\bar{y}_{a..b}$ is the empirical mean of the sub-signal $y_{a..b}$.

3.3 Feature extraction

After segmentation, descriptive features are extracted from the full signal and each subsegment. To characterize signal behavior, a compact set of features is computed, including the maximum, minimum, mean, median, sum, sum of squares, and segment length. These features capture the essential amplitude, distribution, and energy characteristics of the signal, avoiding unnecessary complexity that would result in overfitting by making the feature space too big. These features are calculated for each segment, as well as for the entire signal, resulting in seven features per segment and per sensor signal.

To benchmark the benefits of change-point-based segmentation, a second feature set is generated using fixed, uniformly sized segments whose boundaries are defined beforehand. This enables direct comparison of adaptive and non-adaptive segmentation strategies.

To further improve the results of the prediction, additional metadata could be used as features. But in this study, only the features from the time series should be considered.

3.4 Machine learning model

A supervised ML model is trained based on the extracted process features to predict the resulting tensile shear force of the welded joint. In this regression task, the feature set serves as the model input, and the tensile shear strength acts as the target variable.

3.4.1 Model choice

Given the requirements for a regression model that is robust, computationally efficient, and partially interpretable, an ensemble method based on decision trees was selected. Specifically, the ExtraTreesRegressor (Extremely Randomized Trees) is used [23]. Decision-tree-based models are well-suited for heterogeneous feature sets and nonlinear relationships, offering the following advantages:

They perform hierarchical, rule-based splits that naturally capture complex interactions in the data. They require minimal preprocessing and scaling of numerical features. They provide built-in feature importance measures.

However, single decision trees tend to overfit. The Extra Trees algorithm mitigates this issue by creating an ensemble of decorrelated trees where feature selection and split thresholds are strongly randomized. This reduces variance, improves generalization, and results in faster training than classical tree ensembles, such as Random Forests.

Previous work, including that of Müller et al. [9], has shown that Extra Trees achieves high predictive accuracy for ultrasonic welding applications. This makes the method a well-founded choice.

3.4.2 Pipeline and hyperparameters

Model training is implemented entirely using the *scikit-learn* framework [24]. The training procedure is embedded in a structured ML pipeline. Numerical features are standardized. The estimator itself is configured as follows:

- ExtraTreesRegressor
- 500 estimators
- Maximum tree depth: 20
- Minimum samples per split: 2

These hyperparameters represent a compromise between model complexity, training time, and predictive accuracy. A moderate number of trees and a restricted maximum depth ensure efficient training while maintaining sufficient expressive power to capture the relevant process dynamics.

The dataset obtained from the experiments is split into training and test sets. To ensure robust validation, a ShuffleSplit cross-validator with five random permutations of the data is used. This allows the model's performance to be evaluated across multiple train-test combinations.

3.4.3 Performance metrics

Model performance is quantified using three standard regression metrics:

- Coefficient of determination R^2, measuring explained variance

- Mean absolute error (*MAE*), representing the average magnitude of prediction errors
- Root mean squared error (*RMSE*), penalizing larger errors more strongly due to the squared term

These complementary metrics evaluate accuracy and deviation from the true tensile shear strengths measured.

3.4.4 Feature selection and importance

To analyze and reduce the feature set, as well as increase interpretability, feature importance is estimated using permutation importance. In this approach, each feature is randomly permuted multiple times (50 times in this study) while all other features remain unchanged. Disrupting the information content of a single feature and measuring the resulting decrease in the model's performance (quantified via R^2) directly assesses how much the model relies on that feature to make accurate predictions. Features whose permutation causes a significant decrease in performance are considered highly influential. Features with little or no impact are considered less important and can be removed from the model [25].

Based on these importance values, the top n features (n = 15, 50, or 100 in the experiments) are selected and passed to the final Extra Trees pipeline. This procedure identifies the most influential signal segments and characteristics, thereby improving transparency and reducing computational effort.

In addition to individual feature importance, grouped permutation importance is evaluated. This method measures the predictive contribution of entire feature groups rather than single variables. For each group, all contained features are permuted simultaneously and the resulting change in model performance is measured. A larger performance drop indicates a higher collective importance of the corresponding group [26, 27].

In this study, feature groups are defined according to sensor type and signal segment. This grouping enables the identification of which sensors contribute most strongly to the prediction and which temporal process phases contain the most relevant information, thereby supporting a physically interpretable analysis of the welding process. This is particularly relevant for change-point-based segmentation, as it allows the predictive relevance of individual welding phases to be assessed directly.

4 Results and discussion

This section first presents the experimental welding results and the resulting variability of the dataset. Subsequently, the influence of adaptive change-point-based segmentation on weld quality prediction is evaluated. Overall, the analysis demonstrates that adaptive segmentation improves prediction accuracy compared to non-segmented signals and achieves optimal performance with a compact number of physically meaningful segments.

Table 4 summarizes the descriptive statistics of the tensile shear forces obtained for all investigated test groups.

The achieved shear force of the joint exhibits a clear dependence on the respective test series. The reference condition (R) yields a mean shear force of 2553 N with a standard deviation of 261 N. The relatively large range (2255 N) and the presence of 16 statistical outliers indicate occasional low-strength welds, which is also reflected by the low minimum value (1043 N).

Table 4 Descriptive statistics of all groups

Test series	Count [-]	Mean [N]	Median [N]	Std. Dev. [N]	Min [N]	Max [N]	Range [N]	Outliers [-]
R	476	2553	2568	261	1043	3297	2255	16
S	221	2186	2181	130	1852	2613	761	5
H	126	3029	3079	248	2007	3516	1509	1
F	246	2250	2271	316	1227	2960	1733	3
C	75	2563	2528	220	2184	3449	1265	1
A	45	2209	2184	368	1331	3011	1680	0
X	42	2220	2265	198	1663	2635	972	1
O	41	2400	2369	288	1717	3003	1286	0
Total	1272	2450	2429	356	1043	3516	2473	20

Chemically cleaned specimens (C) show a comparable mean shear force (2563 N), with slightly reduced variability (220 N) and only one detected outlier. The narrower range (1265 N) compared to the reference group suggests a more homogeneous process behavior.

The hardness series (H) achieves the highest mean (3029 N) shear forces. Despite a broad range of 1509 N, only one outlier is detected, indicating robust and stable joint formation for the harder base material. The elevated minimum value (2007 N) further underlines the consistently high strength level in this group.

Reduced strength levels are observed for the soft material condition (S), the roughened specimens (A), and the contaminated condition (F). The soft material group exhibits a low mean shear force of 2186 N but also the smallest standard deviation (130 N) and the narrowest range (761 N), indicating comparatively uniform but reduced joint strength.

In contrast, the roughened specimens (A) and contaminated specimens (F) show larger scatter (368 N and 316 N, respectively) and wider ranges. The contaminated group (F) exhibits three outliers and a low minimum value (1227 N), highlighting the detrimental and less predictable effect of surface contamination on joint performance.

Specimens welded without clamping (X) show a decreased mean shear force (2220 N) with moderate variability (198 N) and one outlier. The reduced minimum value (1663 N) compared to the reference condition indicates the sensitivity of the process to insufficient mechanical fixation.

The overall dataset results in a mean shear force of 2450 N. The comparatively large overall standard deviation (356 N) and range (2473 N) reflect the combined variability introduced by the different material conditions and process variations investigated.

Figure 4 shows the preprocessed time-series data from the shear force sensor. The signals display pronounced variations both between different weld groups and within individual groups. Furthermore, signal shape and magnitude differ substantially even at identical nominal settings, although the two parameter sets remain distinguishable in the sensor response. Parameter set 2 exhibits higher amplitudes and shorter durations, which can be attributed to the increased welding pressure, resulting in larger anvil motion, and to the lower applied welding energy. The remaining sensor signals are shown in Fig. 10. These observations confirm that the dataset contains meaningful process disturbances and underline the necessity of advanced feature extraction methods capable of capturing phase-dependent signal behavior.

As a baseline, weld quality prediction was first performed using features extracted from the complete, non-segmented signals. The results are shown in Fig. 5.

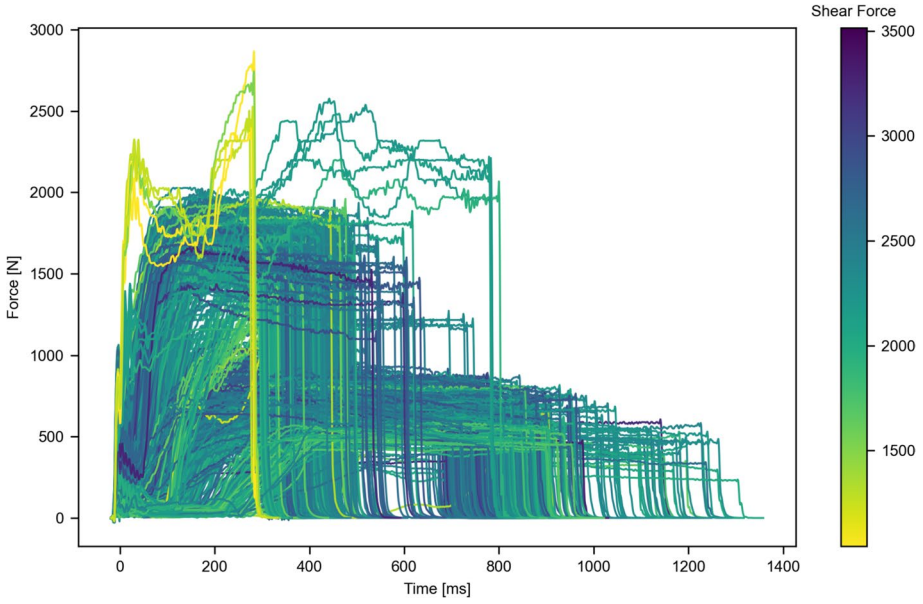

Fig. 4 Preprocessed time series for the shear force sensor with the corresponding resulting tensile shear strength

Table 5 Prediction result for non-segmented features

Segmentation approach	Data size	Segments	MAE [N]	R^2	RMSE [N]
–	(1272, 54)	1	139.2 ± 9.7	0.70 ± 0.040	190.9 ± 16.2

Table 6 Comparison of the prediction quality from 2 to 10 fixed segments

Segmentation approach	Data size	Segments	MAE [N]	R^2	RMSE [N]
Fixed	(1272, 100)	9	130.1 ± 9.5	0.748 ± 0.033	176.0 ± 14.3
Fixed	(1272, 50)	5	130.4 ± 9.5	0.738 ± 0.035	179.4 ± 14.6
Fixed	(1272, 100)	10	130.6 ± 8.5	0.740 ± 0.034	178.4 ± 14.0
Fixed	(1272, 100)	8	130.9 ± 9.3	0.746 ± 0.030	176.7 ± 13.0
Fixed	(1272, 100)	6	131.0 ± 9.8	0.738 ± 0.036	179.2 ± 14.8

Shown are the five best results for this approach

The data set comprises 1272 welds, each with 54 features, calculated from nine extracted time series, each with six features. The segment length, the seventh feature, is not calculated for the whole signal. While this approach already yields reasonable prediction accuracy, the performance indicates that important temporal information is lost when the signal is treated as a single segment. This confirms that segmentation is necessary to capture the phase-dependent dynamics of the welding process.

A total of 220 different model configurations were evaluated, varying segmentation approach, number of segments, feature subset size, and reference signal for hybrid segmentation.

Table 6 summarizes the best results obtained using fixed equal-length segmentation. The results show that increasing the number of fixed segments improves predictive accuracy up to approximately eight to ten segments. This behavior indicates that

Table 7 Comparison of the prediction quality for different number of segments

Segmentation approach	Data size	Segments	MAE [N]	R^2	RMSE [N]
Hybrid (Shear force sensor)	(1272, 50)	3	128.5 ± 7.1	0.751 ± 0.027	174.7 ± 9.7
Hybrid (Shear force sensor)	(1272, 50)	4	136.4 ± 8.7	0.722 ± 0.036	184.6 ± 14.3
Hybrid (Shear force sensor)	(1272, 50)	6	136.4 ± 9.1	0.724 ± 0.032	184.0 ± 13.0
Hybrid (Shear force sensor)	(1272, 50)	5	138.4 ± 10.9	0.709 ± 0.043	188.8 ± 17.4
Hybrid (Shear force sensor)	(1272, 50)	2	138.7 ± 9.6	0.707 ± 0.039	189.7 ± 15.7

Table 8 Comparison of the prediction quality for different data sizes

Segmentation approach	Data size	Segments	MAE [N]	R^2	RMSE [N]
Hybrid (Shear force sensor)	(1272, 50)	3	128.5 ± 7.1	0.751 ± 0.027	174.7 ± 9.7
Hybrid (Shear force sensor)	(1272, 100)	3	130.1 ± 8.3	0.747 ± 0.034	176 ± 11.5
Hybrid (Shear force sensor)	(1272, 219)	3	132.4 ± 8.8	0.739 ± 0.037	178.7 ± 12.5
Hybrid (Shear force sensor)	(1272, 15)	3	135.3 ± 7.4	0.727 ± 0.025	183.4 ± 10.7

Table 9 Comparison of the prediction quality for different segmentation approaches

Segmentation approach	Data size	Segments	MAE [N]	R^2	RMSE [N]
Hybrid (Shear force sensor)	(1272, 50)	3	128.5 ± 7.1	0.751 ± 0.027	174.7 ± 9.7
Univariate	(1272, 50)	3	128.9 ± 7.9	0.743 ± 0.028	177.7 ± 12.5
Multivariate	(1272, 50)	3	131.8 ± 8.4	0.739 ± 0.025	179.0 ± 10.6

dividing the signal into multiple temporal regions enables the extraction of additional predictive information. However, the comparatively large number of required segments suggests that fixed segmentation distributes informative process transitions across artificial boundaries and therefore requires finer subdivision to capture relevant dynamics. In addition, the use of fixed segment boundaries complicates the interpretation of feature importance, as relevant signal characteristics may be split across different segments, preventing a consistent assignment of influential features to specific physical process phases.

Table 7 compares prediction performance for different numbers of segments obtained using change-point-based hybrid segmentation. The results demonstrate that three segments provide the best predictive accuracy. Using fewer segments fails to capture important process transitions, whereas increasing the number of segments leads to a gradual reduction in performance. This behavior indicates oversegmentation, which increases feature dimensionality and sensitivity to noise while reducing generalization capability.

Notably, adaptive segmentation achieves optimal performance with substantially fewer segments than the fixed approach. This indicates that change point detection concentrates informative signal transitions into a compact set of statistically derived temporal regions that align more closely with the physical welding progression.

Table 8 compares prediction performance for different numbers of selected features. Intermediate feature subset sizes consistently provide the highest predictive accuracy. While the results are shown here for the hybrid approach, all other segmentation approaches also achieve their best performance with 50 selected features. Very large feature sets slightly reduce performance due to overfitting, whereas strongly reduced

feature sets fail to capture sufficient process information. This confirms that permutation-importance-based feature selection provides an effective balance between information content and model complexity.

Table 9 compares the three investigated segmentation strategies. The hybrid change-point-based approach consistently achieves the highest predictive accuracy. Univariate segmentation yields slightly lower performance, while fully multivariate segmentation performs similarly but requires substantially higher computational effort. The superior performance of the hybrid approach indicates that selecting a physically meaningful reference signal enables robust identification of relevant process transitions while maintaining computational efficiency. Overall, the best-performing configuration uses three segments and a feature subset of 50 features with the hybrid approach based on the shear force sensor. Compared with the fixed segmentation approach, the predictive performance improves only marginally. However, the primary advantage lies in the markedly enhanced interpretability and improved transferability to new welding setups or process conditions, as the segmentation aligns with physically meaningful process stages rather than dataset-specific time partitions. Based on these results, this configuration is examined in greater detail in the subsequent analysis.

Figure 5 shows the relationship between predicted and measured tensile shear forces for one representative cross-validation split, with data points colored according to the respective test group. The predictions closely follow the diagonal reference line, indicating good agreement between predicted and measured values across the full strength range. No systematic deviation is visible for individual welding conditions, suggesting that the model generalizes well across different material states and process disturbances.

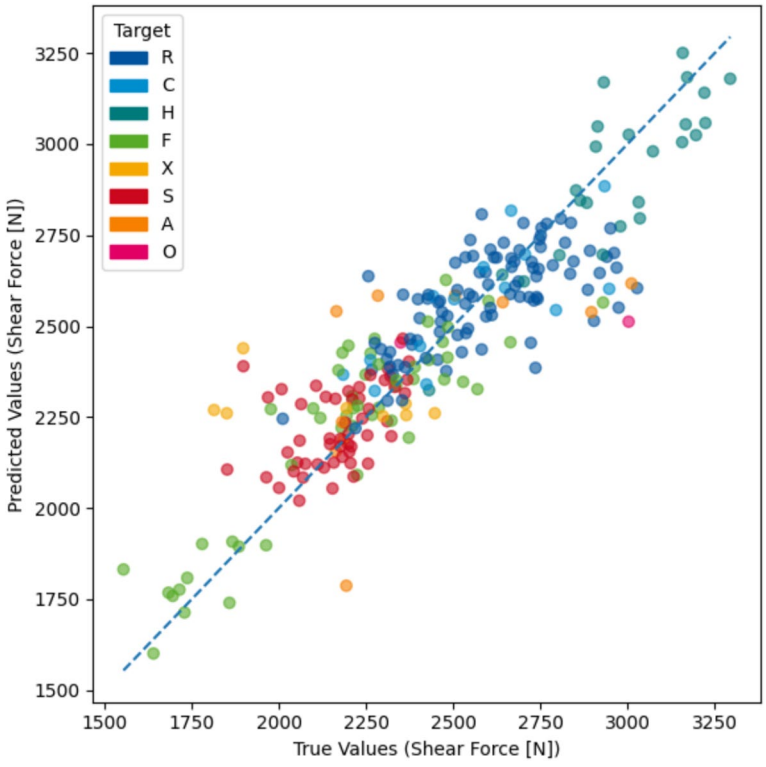

Fig. 5 Predicted versus measured tensile shear force for one representative cross-validation split for the hybrid change-point-based approach. Points are colored according to the test group, and the dashed line indicates perfect agreement ($R^2 = 0.784$, $MAE = 116.8N$)

Table 10 Mean absolute error (MAE) of the predicted tensile shear force for each test group

Test series	MAE [N]
R	127.7
S	102.7
H	126.6
F	127.3
C	131.4
A	187.0
X	137.5
O	209.8

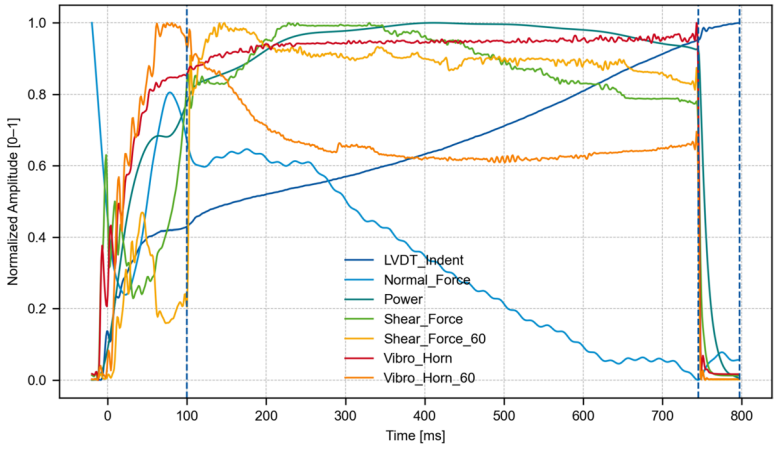

Fig. 6 Processed sensor signals for an exemplary weld from the reference group with added segmentation for the three segment hybrid approach

The remaining deviations are primarily observed for groups with higher intrinsic variability and smaller sample sizes, consistent with the subgroup error analysis. The corresponding scatter plots for the remaining four cross-validation splits are provided in the appendix and show comparable prediction behavior.

To further assess model robustness across different welding conditions, the prediction error was evaluated separately for each test group. The resulting mean absolute errors are summarized in Table 10. The error remains relatively consistent for the majority of groups, including the reference condition (R), cleaned specimens (C), hardened material (H), contaminated samples (F), and unclamped welds (X), all showing MAE values in the range of approximately 125 to 140 N. The soft material condition (S) exhibits an even lower error level, indicating a particularly consistent relationship between sensor signals and the resulting joint strength for this group.

In contrast, substantially higher prediction errors are observed for the roughened specimens (A) and the group with other conditions (O), with MAE values close to 190 N and 210 N, respectively. These groups exhibit comparatively large standard deviations in tensile shear force (Table 4), indicating increased internal variability and less uniform welding behavior. In addition, both groups contain only a small number of samples, which reduces the statistical representativeness of the training data and increases sensitivity to individual weld deviations. Such heterogeneous process conditions and limited

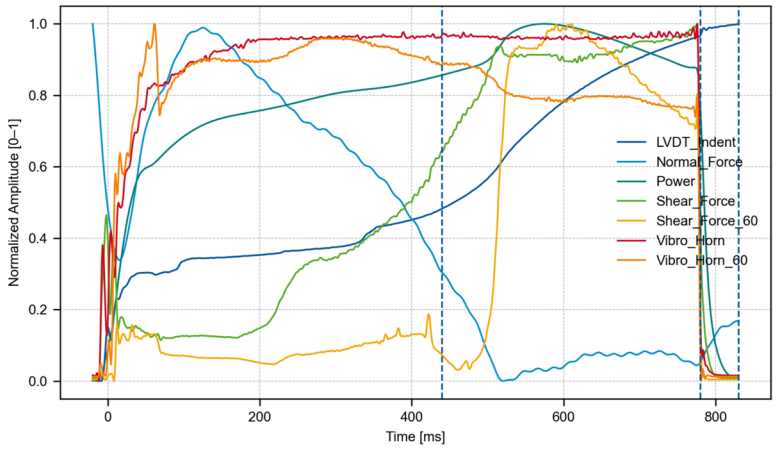

Fig. 7 Processed sensor signals for an exemplary weld from the contaminated group with added segmentation for the three segment hybrid approach

sample sizes lead to weaker and less deterministic relationships between sensor signals and joint strength, thereby increasing prediction uncertainty.

To provide physical context for the segmentation and the resulting feature relevance, Figs. 6 and 7 show representative processed sensor signals for a weld from the reference group and from the contaminated group, respectively, including the detected three-segment hybrid partitioning using the shear force signal.

A comparison between the contaminated weld and the reference weld reveals clear differences in both signal evolution and detected segmentation boundaries. For the reference weld, the first segment ends at approximately 100 ms, whereas for the contaminated weld it extends to roughly 450 ms, indicating a substantially prolonged initial surface interaction phase under contaminated conditions.

While the sonotrode vibrometer signal shows only minor variations between both cases, the shear force signal exhibits pronounced differences, confirming its suitability as the reference signal for segmentation. The contaminated condition reduces friction between the joining partners, which results in lower shear force amplitudes in the anvil during the early welding stage. Only after the surface cleaning phase progresses do the amplitudes increase. The indentation signal also differs considerably, most likely due to the reduced friction and associated lower heat generation, which delays material softening and plastic deformation. Consequently, the contaminated weld shows a slower initial increase in indentation compared to the reference weld. Overall, the reference condition exhibits steeper early signal gradients and therefore transitions earlier into the subsequent process phase. These observations confirm that the detected change-point-based segments correspond to physically meaningful welding stages.

To quantify the predictive relevance of the extracted features, permutation feature importance was evaluated for the best-performing configuration. Figure 8 presents the ranking of the most influential individual features. Because segment indices follow Python-based zero indexing, segment 0 denotes the first temporal welding phase.

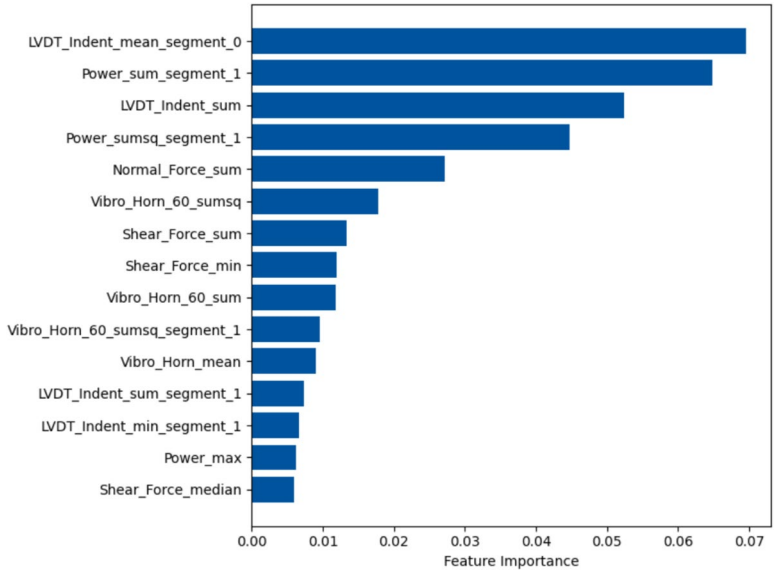

Fig. 8 Permutation feature importance of the best-performing prediction model, showing the 15 most influential features ranked by their mean decrease in prediction performance when permuted

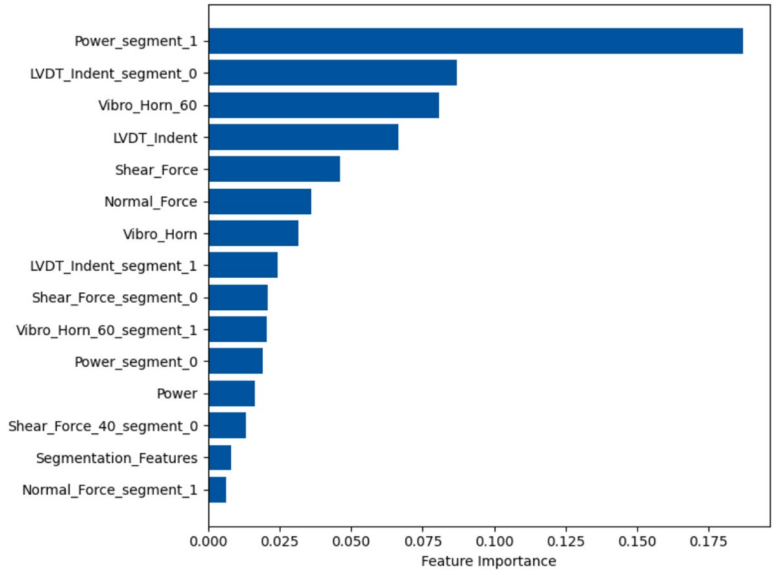

Fig. 9 Grouped permutation feature importance aggregated by sensor type and temporal segment for the best-performing model

The permutation importance ranking is consistent with the observed process behavior. Although features derived directly from the shear force signal are not among the highest-ranked individual predictors, the signal remains fundamentally important because it serves as the reference for change-point detection and therefore defines the segmentation boundaries applied to all sensors. Its contribution to prediction performance is

therefore better understood as largely structural rather than purely feature-specific, since it determines the temporal partitioning of the feature representation.

The most influential individual feature corresponds to the mean indentation value in the first segment, indicating that early material deformation strongly affects the final joint strength. Features derived from the electrical power signal contribute mainly in the second segment, reflecting differences between parameter sets and characteristic variations in energy input. Additional relevance is observed for vibration-related features computed over the entire signal duration, indicating that both localized phase behavior and global signal characteristics contain useful predictive information.

Figure 9 presents the grouped permutation importance aggregated by sensor type and temporal segment. The electrical power signal in segment 1 shows the highest grouped relevance, followed by indentation-related features in segment 0. This shows that different physical welding stages are characterized by different dominant sensor contributions. Features derived from the shear force signal and from the third harmonic of the vibrometer signal show strong importance primarily when computed over the entire signal rather than individual segments. This is reflected both in the individual feature ranking and in the grouped permutation analysis. Overall, features derived from the electrical power, indentation, and vibration signals show the highest predictive relevance, whereas the normal force signal and especially the second harmonic of the vibration signals contribute comparatively less to the prediction.

In addition to model performance metrics, part of the remaining prediction error can be attributed to inherent process variability and measurement uncertainty, commonly referred to as error of variance (EOV) (see [28]). These effects arise from sensor noise, material batch variations, temperature fluctuations, uncertainties in mechanical testing, and other uncontrolled external influences that cannot be fully captured by the available sensor signals. Consequently, even an optimal model cannot eliminate this residual variance entirely.

5 Conclusion and outlook

This study introduced an adaptive change-point-based segmentation framework for machine-learning-based weld quality prediction in ultrasonic metal welding.

The results demonstrate that statistically derived segmentation improves the extraction of informative temporal features compared to conventional equal-length segmentation. By identifying intrinsic transitions in the sensor signals, the proposed method generates compact segment representations that reflect the phase-dependent dynamics of the welding process. This structured representation not only improves predictive performance but also substantially enhances model interpretability and facilitates transferability to new welding setups or process conditions, since the segmentation aligns with physically meaningful process stages rather than dataset-specific time partitions.

Among the investigated strategies, the hybrid segmentation approach, in which change points are determined from a physically meaningful reference signal (shear force signal in the anvil) and applied consistently across all sensors, provides the best compromise between predictive accuracy, robustness, and computational efficiency. Furthermore, the segment-based feature representation enables direct attribution of predictive relevance to specific welding stages, significantly enhancing model interpretability compared to conventional time-series feature extraction.

Although the present study relies on offline change-point detection to ensure stable segmentation during model development, the remaining components of the processing pipeline are computationally lightweight and suitable for real-time implementation. Future work will therefore focus on online or approximate segmentation strategies that allow adaptive feature extraction during the welding process. This would enable weld quality predictions prior to process completion and represents an important step toward fully in-line industrial monitoring.

Overall, the presented methodology demonstrates that combining statistical signal segmentation with domain-specific process knowledge provides a transparent and practically applicable foundation for reliable data-driven weld quality monitoring in ultrasonic metal welding.

Appendix

Measurement data

In Fig. 10, the processed measurement data of the sensors is shown. For the shear force and vibrometer at the sonotrode, three different bandpass filters at the higher harmonics are applied, resulting in three different time series data for these sensors.

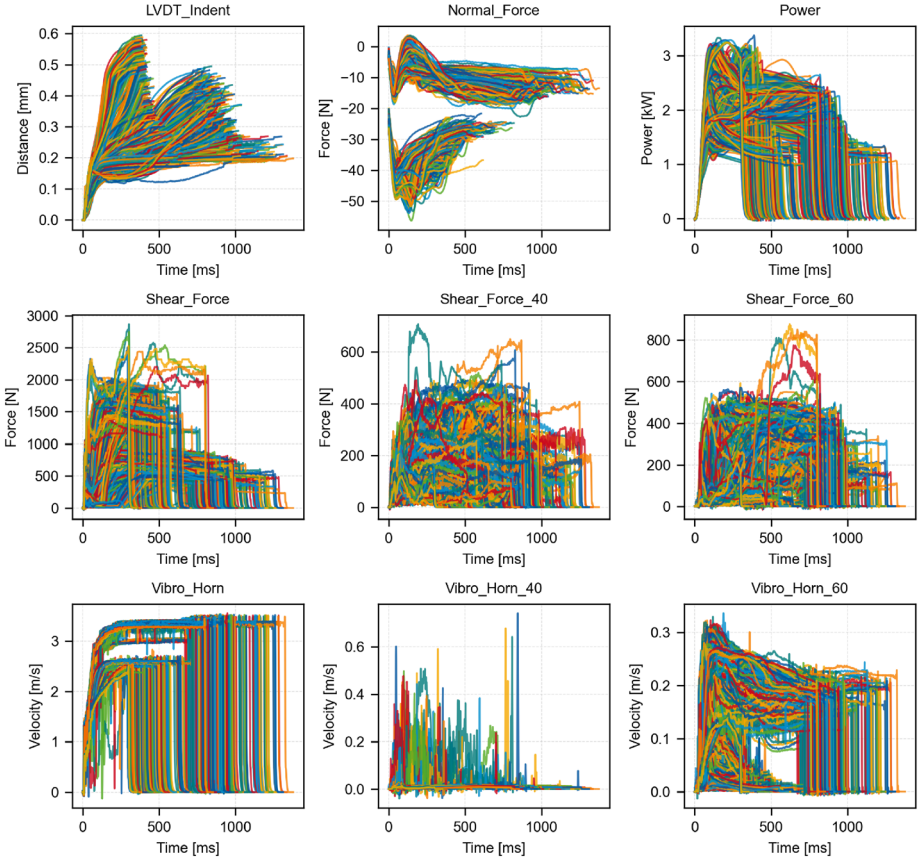

Fig. 10 Measurement data of the six sensors

Scatter plots

The following figures show predicted versus measured tensile shear forces for the remaining four cross-validation splits corresponding to the representative example shown in Fig. 5.

See Figs. 11, 12, 13, and 14

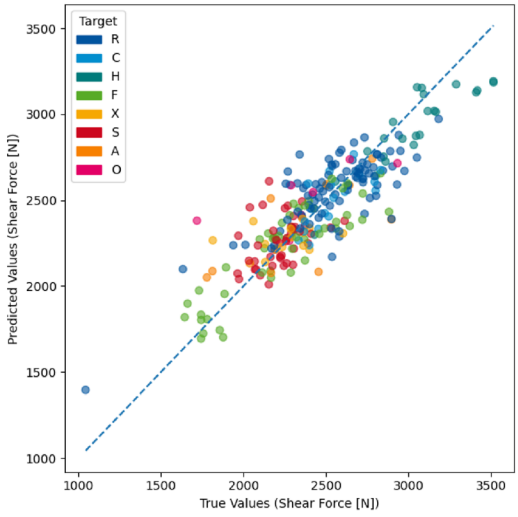

Fig. 11 Predicted versus measured tensile shear force for cross-validation split 2 for the hybrid change-point-based approach

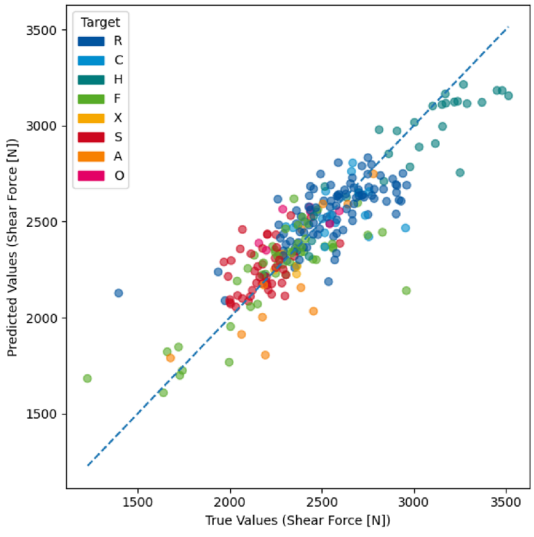

Fig. 12 Predicted versus measured tensile shear force for cross-validation split 3 for the hybrid change-point-based approach

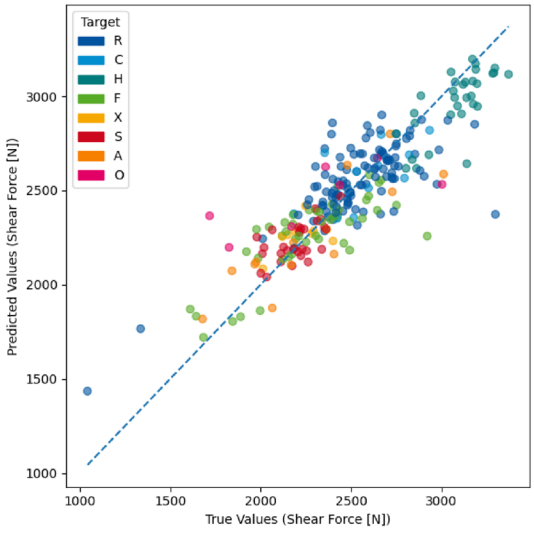

Fig. 13 Predicted versus measured tensile shear force for cross-validation split 4 for the hybrid change-point-based approach

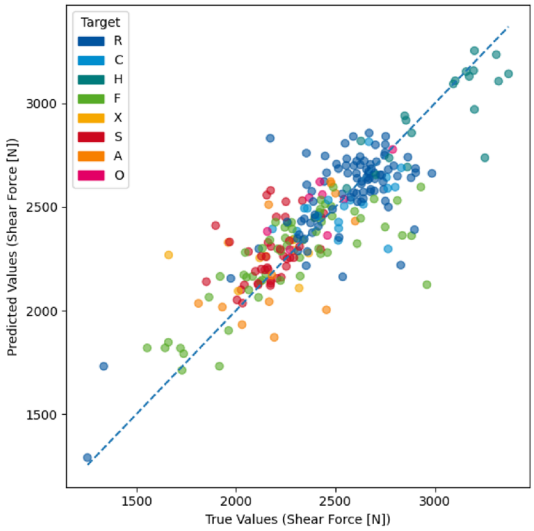

Fig. 14 Predicted versus measured tensile shear force for cross-validation split 5 for the hybrid change-point-based approach

Author contributions
All authors contributed to the study conception and design. Material preparation and data collection were performed by E. Helfers. Data analysis and correlation were performed by O. Stockemer. The first draft of the manuscript was written by O. Stockemer and E. Helfers. All authors commented on previous versions of the manuscript. All authors read and approved the final manuscript.

Funding
Open Access funding enabled and organized by Projekt DEAL. Funded by the Deutsche Forschungsgemeinschaft (DFG-German Research Foundation) under Grant Number 520475171 "Hybrid Process Prediction for Ultrasonic Metal Welding-Pro2MUSS".

Data availibility
Data will be made available on reasonable request by the corresponding author.

Code availability
Code will be made available on reasonable request by the corresponding author.

Materials availability
Not applicable.

Declarations

Ethics approval and consent to participate
Not applicable.

Consent for publication
Not applicable.

Competing interests
The authors declare no competing interests.

Received: 30 November 2025 / Accepted: 13 March 2026
Published online: 26 March 2026

References

1. European Comission: Communication from the commission to the european parliament, the european council, the council, the european economic and social committee and the committee of the regions, the european green deal: 52019DC0640. 2019. https://eur-lex.europa.eu/legal-content/EN/TXT/?uri=COM%3A2019%3A640%3AFIN.
2. Vries E. Mechanics and mechanisms of ultrasonic metal welding dissertation. 2004. http://rave.ohiolink.edu/etdc/view?acc_num=osu1078415529 Accessed 26 Jan 2025.
3. Balz I. Prozessanalyse der Thermo-mechanischen Vorgänge Während der Verbindungsbildung Beim Metall-Ultraschallschweißen // Analysis of Thermo-mechanical Processes During the Bond Formation in Ultrasonic Metal welding, 1. auflage edn. Aachener Berichte Fügetechnik, vol. 2020,3. Shaker, Düren 2020. https://doi.org/10.18154/RWTH-2020-08744
4. Gallego-Juárez JA, Graff KF, Lucas M, editors. Power ultrasonics: applications of high-intensity ultrasound. Second edition edn: Woodhead Publishing series in electronic and optical materials. Woodhead Publishing, Oxford; 2022. https://doi.org/10.1016/C2019-0-00783-2.
5. Helfers E, Müller FW, Schiebahn A, Reisgen U. Influence of surface condition of copper sheets on ultrasonic metal welding. J Adv Join Process. 2024;9:100204. https://doi.org/10.1016/j.jajp.2024.100204.
6. Wodara J, Adam T. Ultraschallfügen und -trennen, vol. 1. Düsseldorf: der Grundlagen der Fügetechnik. DVS Verlag; 2004.
7. Müller FW, Schiebahn A, Reisgen U. Quality prediction of disturbed ultrasonic metal welds. J Adv Join Process. 2022;5:100086. https://doi.org/10.1016/j.jajp.2021.100086.
8. Pöthig P, Grätzel M, Bergmann JP. Influence of different surface conditions on mechanical properties during ultrasonic welding of aluminum wire strands and copper terminals. Weld World. 2023;67(6):1427–36. https://doi.org/10.1007/s40194-023-01490-x.
9. Müller FW, Mirz C, Schiebahn A, Reisgen U. Influence of quality features, disturbances, sensor data, and measurement time on quality prediction for ultrasonic metal welding. Weld World. 2025. https://doi.org/10.1007/s40194-025-01959-x.
10. Klobčar D, Tušek J, Bizjak M, Leser V. Micro friction stir welding of copper electrical contacts. Metalurgija -Sisak then Zagreb-. 2014;47911:620–172.
11. Schwarz EB, Bleier F, Guenter F, Mikut R, Bergmann JP. Improving process monitoring of ultrasonic metal welding using classical machine learning methods and process-informed time series evaluation. J Manuf Process. 2022;77:54–62. https://doi.org/10.1016/j.jmapro.2022.02.057.
12. Müller FW, Mirz C, Weil S, Schiebahn A, Corves B, Reisgen U. Weld quality characterization by vibration analysis for ultrasonic metal welding processes. J Adv Join Process. 2023;8:100149. https://doi.org/10.1016/j.jajp.2023.100149.
13. Xu R, Song Z, Wu J, Wang C, Zhou S. Change-point detection with deep learning: a review. Front Eng Manag. 2025;12(1):154–76. https://doi.org/10.1007/s42524-025-4109-z.
14. Helfers E, Stockemer O, Müller FW, Schiebahn A, Reisgen U, Corves B. Shear force sensors for process monitoring in ultrasonic metal welding–design, calibration, and validation. Weld World. 2025. https://doi.org/10.1007/s40194-025-02221-0.
15. Feldman M. Hilbert transform in vibration analysis. Mech Syst Signal Process. 2011;25(3):735–802. https://doi.org/10.1016/j.ymssp.2010.07.018.
16. Hastie T, Tibshirani R, Friedman JH. The elements of statistical learning: data mining, inference, and prediction, 2. ed., corr. at 4. print edn. Springer series in statistics. Springer, New York, NY 2009. https://doi.org/10.1007/978-0-387-84858-7.
17. Page ES. A test for a change in a parameter occurring at an unknown point. Biometrika. 1955;42(3/4):523–7.
18. Jandhyala V, Fotopoulos S, MacNeill I, Liu P. Inference for single and multiple change-points in time series. J Time Ser Anal. 2013;34(4):423–46. https://doi.org/10.1111/jtsa.12035.
19. Li J, Fearnhead P, Fryzlewicz P, Wang T. Automatic change-point detection in time series via deep learning. J R Stat Soc Ser B Stat Methodol. 2024. https://doi.org/10.1093/jrsssb/qkae004.
20. Lee W-H, Ortiz J, Ko B, Lee R. Time series segmentation through automatic feature learning. 2018. https://arxiv.org/pdf/1801.05394.
21. Lattari F, Rucci A, Matteucci M. A deep learning approach for change points detection in inSAR time series. IEEE Trans Geosci Remote Sens. 2022;60:1–16. https://doi.org/10.1109/TGRS.2022.3155969.
22. Truong C, Oudre L, Vayatis N. Selective review of offline change point detection methods. Signal Process. 2020;167:107299. https://doi.org/10.1016/j.sigpro.2019.107299.
23. Geurts P, Ernst D, Wehenkel L. Extremely randomized trees. Mach Learn. 2006;63(1):3–42. https://doi.org/10.1007/s10994-006-6226-1.

24. Pedregosa F, Varoquaux G, Gramfort A, Michel V, Thirion B, Grisel O, et al. Scikit-learn: machine learning in python. 2011. http://arxiv.org/pdf/1201.0490.
25. Molnar C. Interpretable machine learning: a guide for making black box models explainable, 3rd ed. 2025. https://christophm.github.io/interpretable-ml-book.
26. Plagwitz L, Brenner A, Fujarski M, Varghese J. Supporting ai-explainability by analyzing feature subsets in a machine learning model. Stud Health Technol Inform. 2022;294:109–13. https://doi.org/10.3233/SHTI220406.
27. Au Q, Herbinger J, Stachl C, Bischl B, Casalicchio G. Grouped feature importance and combined features effect plot. Data Min Knowl Disc. 2022;36(4):1401–50. https://doi.org/10.1007/s10618-022-00840-5.
28. Rezazadeh N, Luca A, Perfetto D, Salami MR, Lamanna G. Systematic critical review of structural health monitoring under environmental and operational variability: approaches for baseline compensation, adaptation, and reference-free techniques. Smart Mater Struct. 2025;34(7):073001. https://doi.org/10.1088/1361-665X/ade7db.